Industrial Engineering Journal
ISSN: 0970-2555
Volume : 52, Issue 3, March : 2023

TOPOLOGY OPTIMIZATION IN 3D AND TISSUE ENGINEERING

T.K Bhanj, S. Joshi, A. Nanda, S. P. Baral, S. Sharma, Basic science and humanity, AIET Bhubaneswar

Abstract: - The advancement in the designing and fabrication technique solved many problems related to optimized microstructure and defects. The additive manufacturing is one of the most advance technologies successfully applied in manufacturing sector. In material science, all types of designs can be possible in AM. The crucial part of the AM is topology optimization. The designs are prepared for certain purpose must mimic the surrounding environment and can be adjustable. The topology are the building block of the design to accomplish the optimize task. The fabrication of various designs by AM for orthopedic application is a crucial part of tissue engineering. The living beings consist of both hard and soft tissue ranging from micro to nano level. So the development of the regenerative medicine is a big challenge. In this review, the latest advancement in different aspects of the design and manufacturing of additively manufactured metallic biomaterials are highlighted. Then, we elaborate on the tools and approaches undertaken for the design of scaffold with engineered internal architecture including, topology optimization techniques, as well as unit cell patterns based on lattice networks.

Key words**:** Topology. Simulation, Additive manufacturing, compliance

1. **Introduction-**Topology optimization is one among mathematical forms that optimizes material layout within a given design space, for a given set of loads and boundary conditions such that the layout forms perform the target objective [1]. Topology optimization is used at the concept level of the design process to arrive at a conceptual design proposal that is then fine-tuned for performance and manufacturability. By using topological optimization, the scientists can find the best concept design that meets the design requirement. It reduces the time consuming and design iterations. This results the design development time and overall cost during the development of design performance. Most of the topology optimization designs are complicated in nature that makes it very difficult to manufacture using conventional methods of manufacturing. Very often the production coat can be reduced by different type of material selection analysis [2]. But the advantage of the AM is the wastage of material is very less and only the amount of material required for production of part is used. In Additive manufacturing process the material is spread on the building bed in layer-by-layer fashion and sintered by various methods to get a optimized product bottom up. In particular the process of additive manufacturing could not be come to existence without the computer tool ‘computer aideddesign (CAD)[3].In case of the fabrication of the implants for orthopedic application the material selection and their characterization through various mathematical tools is important before reaching the mass production to reduce the production coast and easy accessibility. There various topological optimization is used to optimize the product quality for the traumatic applications. In this paper the topologies which most frequently used in AM are briefly explained.

1.1 solid isotropic materials with penalization (SIMP) technique

As mentioned above, the solid isotropic material with penalization (SIMP) method is the most widely used approach for topology optimization in biomedical applications [4]. The SIMP approach is a gradientbased approach that utilizes a power-law relationship to establish the material properties as functions of a pseudo-density design variable. The design domain is discredited to finite elements with a pseudo-density design variable assigned to every element. The collective pseudodensity variables become the design

variables. In essence, the number of finite elements in the discretized model defines the number of design variables. Most algorithms are based on minimizing the compliance (maximizing the stiffness) of the structure while placing a constraint on the material volume. Mathematically, the problem can be expressed according to the following definitions:

Objective function (Eq^n 1):

Minimize C= F^TU =U^TKU =$\sum_{e=1}^{n} E_e(\rho_e) u^T k_o$u

Finite element or structural analysis(eq^{n}2)

K(ρ)U(ρ) = F

Volume constraint (Eq^n 3) $\frac{\sum_{e=1}^{n} V(\rho_e)}{fV_o} \leq 1$

Pseudo-density variable constraint (Eq^{n}4)

$0 \leq \rho_e \leq 1$

Where C = Compliance

F= force U =Displacement response

E = Young's modulus (Elastic modulus)

K= stiffness

V= Volume

F= Volume fraction

ρ= Pseudo-density design variables of the design problem

V_O= Original/initial material volume

k_o= Stiffness of a finite element

u =Elemental displacement

e= Elemental parameter

n= Number of elements in the discretized domain.

The Young's Modulus of every element is given by a power-law expression in Eq^n 5

$E_e(\rho_e) = E_{min} + \rho_e^p (E_O - E_{min})$……. (5)

Where E_O =Young's modulus value of the solid material

E_{min}= Young's modulus value of the void material

P = SIMP penalty value

So, the Compliance derivative (Eq^{n}6)

$\frac{dc}{d\rho} = -U^T(\boldsymbol{\rho}) \frac{dk}{d\rho} U(\boldsymbol{\rho})$

Volume derivative for a mesh with constant elements' volumes throughout the optimization

$\frac{dV(\rho)}{d\rho}$ = v …….(Eq^n 7)

Industrial Engineering Journal
ISSN: 0970-2555
Volume : 52, Issue 3, March : 2023

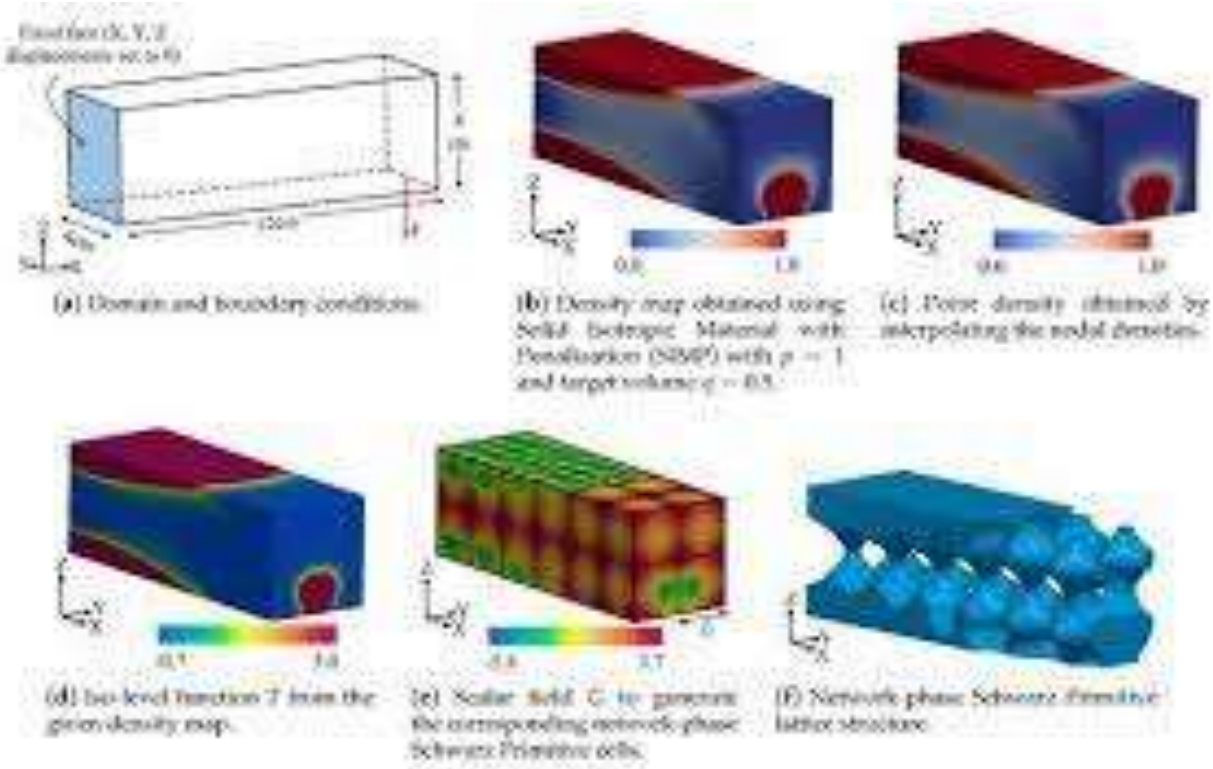

Fig-1The fabrication procedure of by SIMP

1.2 Weighted multi-objective topology optimization

The implant elemeMany implants are subjected to a variety of mechanical loads under a biological-mechanical environment as a result of the several daily activities carried out by the associated physiological region [5]. Each load is taken as a load case that results in unique strain energy or compliance function. Therefore, there are as many strain energy functions as there are loads in this algorithm. To optimize these implants for the loads, a weighted multi-objective topology optimization enables assigning different weights to the strain energy functions with a greater weight given to a load associated with higher functionality. The compliance function in (1) can be rewritten as a consolidated function

Minimize (C =$\sum_I^n w_i \boldsymbol{C_i}$= $\sum_i^n w_i F_i^T \boldsymbol{U_i}$)**….** (**E**q^n 8)

n= 1,2,3, …….

Where w_i is the weight factor of the load

The sensitivity function can be written as

$$\frac{dC}{d\rho} = -\sum_i^n w_i(\boldsymbol{\rho}) \frac{dK}{d\rho} U_i(\boldsymbol{\rho})$$ (Eqn 9)

A multi-objective topology optimizes pelvic prosthesis.

Industrial Engineering Journal
ISSN: 0970-2555
Volume : 52, Issue 3, March : 2023

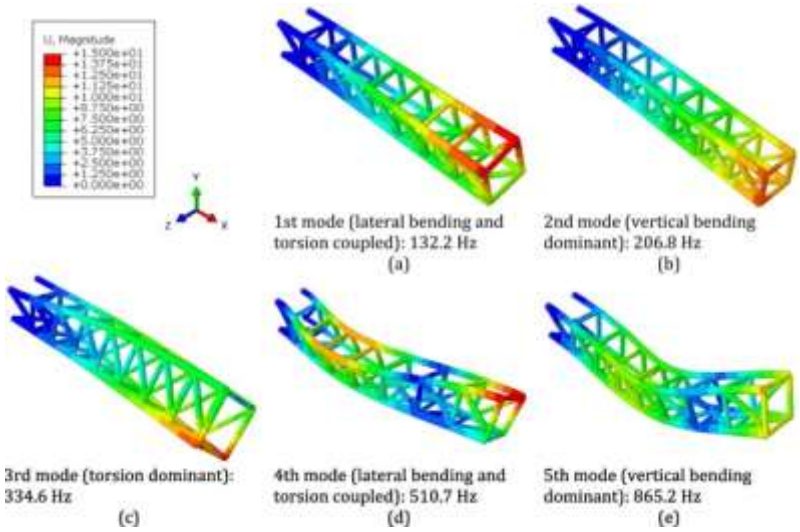

Fig-2 Additive manufacturing by Topological of multi objective topology optimization

1.3 Stress-based topology optimization

In some instances, the optimization is done by minimizing the implant's worst-case state which is failure [6]. Besides, because stress singularity is a possibility when optimal topologies are derived using a different objective function, a stress-based approach can be attractive. Considering the theories of elastic failure, several researchers have attempted to use the maximum distortion energy theory (von Mises) to describe the failure criterion $\sigma_{VM} = \frac{1}{2}\sqrt{\begin{matrix}(\sigma_x^2 - \sigma_y^2)^2 + (\sigma_y^2 - \sigma_z^2)^2 + (\sigma_x^2 - \sigma_z^2)^2 \\ +6\,(\tau_{XY}^2 + \tau_{YZ}^2 + \tau_{ZX}^2)^2\end{matrix}}$ ……..(Eq^n 10)

Obtaining the derivative of Equation (10) with respect to the pseudodensity variable is non-trivial. Additionally, it is very computationally expensive to compute the stress derivative and/or constraint on every element for practical or industrial type designs [30]; therefore, the problem minimization is done on an aggregated maximum stress variable derived by a p-norm function as expressed in Equation (11) [6]:

$\sigma_{vm}^{p-norm} = (\sum_{i=1}^{N}(\frac{\sigma_{VM}}{\sigma_{MAX}})^q)^{\frac{1}{2}}$ …… (Eq^n 11) Where i=1, 2, 3 …….

The objective function and pseudo-density design variable definition of the stress minimization topology optimization problem can then be formulated as Equations (12) and (13):

Minimize σ_{vm}^{p-norm} …… (Eq^n 12)

s.t. $0 < \boldsymbol{\rho} < 1$ ……. (Eq^n 13)

Where σ_{vm}^{p-norm} is the p-norm function of the aggregated maximum stress in the discretized domain

σ_{max} is the maximum allowable stress

'q' is the p-norm power where a higher power results more accurate maximum value but at a significant computational cost.

Industrial Engineering Journal
ISSN: 0970-2555
Volume : 52, Issue 3, March : 2023

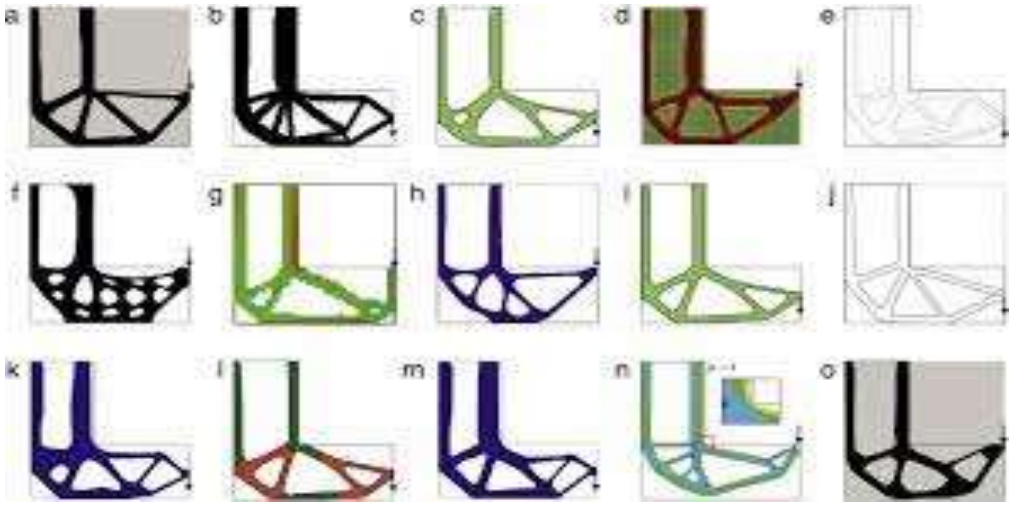

Fig-3 Stress based topological optimization in Additive manufacturing (AM)

1.4. Infill and perimeter control strategies

In a bid to model the venous and porous nature of bone structures, a topology optimization algorithm can be modified by either reformulating the problem statement and/or introducing some constraints. Wu et al. [7] introduced a per-voxel local volume constraint (infill constraint) given in Equations (14) and (15):
{Maximize} for all 'e'

$(\bar{\rho}_e) \approx \bar{\rho}_e = (\sum_e \bar{\rho}_e^q)^{\frac{1}{2}}$ ……. (Eqn 14)

Where $(\sum_e \bar{\rho}_e^q)^{\frac{1}{q}} \leq (\sum_e \alpha^q)^{\frac{1}{q}}$ … (Eqn 15)

By rearranging the equation (12) $(\frac{1}{2}\sum_e \bar{\rho}_e^q)^{\frac{1}{q}} \leq \alpha$ …… (Eqn 16)

ρ_e is the percentage of solid voxels over a given region, while α is the local volume constraint in that region. As mentioned in the previous section, the constraint is a p-norm function that aggregates the maximum local density over the discretized design domain. This function replaces the volume constraint in the conventional problem statement and ensures that the local volume in a specified region is no more than the prescribed local volume, α. In turn, it generates vein-like features throughout the optimized topology. In a similar approach, Park et al. [8] introduced a 'perimeter control' constraint such that a lower bound is placed on the perimeter of every feature. The perimeter function P(ρ), is given in Eqn (17):

$P(\boldsymbol{\rho}) = \int_{\Omega}^{0} |\nabla \rho| d\Omega$

the lower bound on the perimeter is expressed as Eqn (18): $P \geq P_{min}$

where P_{min} is the minimum perimeter value allowed in the final topology. Similar to the local volume constraint, the perimeter control function is added as a constraint, and the derivative is obtained for the optimizer. The resulting topologies after applying local volume constraint and perimeter control constraint.

Industrial Engineering Journal
ISSN: 0970-2555
Volume : 52, Issue 3, March : 2023

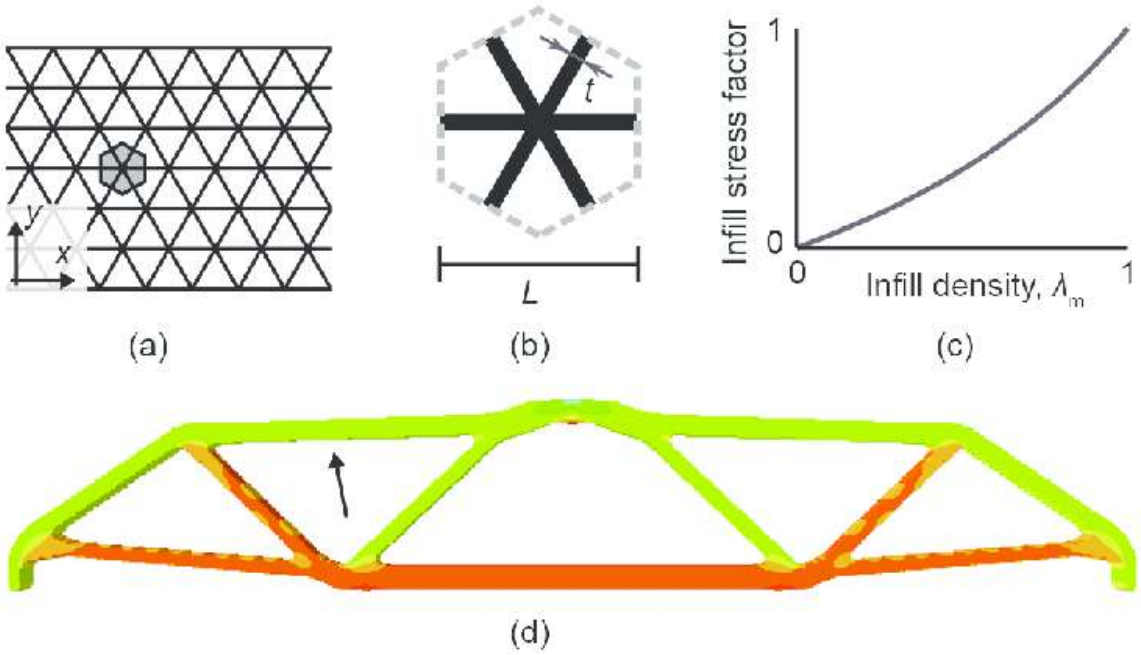

Fig-4 Infill and perimeter control strategies

1.5 Internal pores formation topological optimization

Porous structures can be classified based on their pore interconnectivity (as open and closed pores) as well as the regularity of their pore topology and size (as stochastic and non-stochastic) [9–11]. Ordered pore shapes satisfy the interconnectivity required for cell ingrowth facilitating integration with the host tissue. The porous structures with non-stochastic design involve lattice and TPMS based unit cells [12–15]. To satisfy mechanobiological conformation and reliable integration of the porous implant with host bone tissue, optimization of physical characteristics such as pore shape, pore size, porosity, pore interconnectivity, and micro-topological surface features are required [16]. In the sections below, different types of pore shapes and the relevant tools employed to meet the design requirements for those topologies in metal scaffolds are discussed.

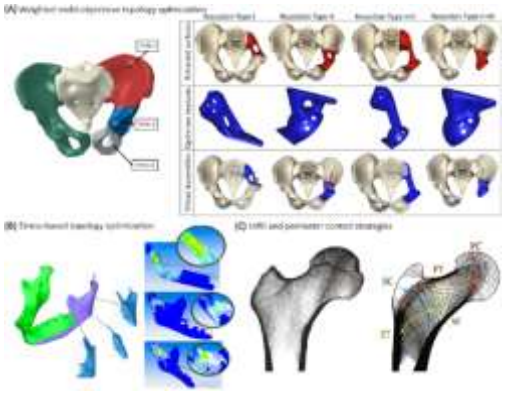

Fig-5 Fabrication of load bearing implant by internal pore formation topology

1.5.1 Stochastic topologies

A stochastic porous structure (known as foam) involves the pores with random shape and size distribution such as those formed using conventional techniques (e.g., salt-leaching and gas-foaming). Despite their random pore distribution, manufacturing parameters could be used to control the pore shape and pore size. Stochastic structures have also been designed for AM via computer modeling and mathematical algorithms. Networked stochastic constructs are defined by a framework consisting of a random joint distribution in a volume. The points are then connected to obtain a connective network and scanned either based on point/pulsing or contour strategy. Voronoi tessellation is another tool for generating stochastic material structures [17,18]. In this method, a set of points (known as seeds) are randomly distributed in the design volume. The space is then partitioned into discrete regions called Voronoi cells [19,20]. Subsequently, a thickness is specified for the edges to form a 3D model [21,22]. Here, the irregularity of the random geometries can be controlled by a tuning factor ε in the range of 0–1 [23]. The native bone microstructure comprises of struts with various thicknesses and nonuniform pore diameters. To better mimic the natural structure of bone, many studies have focused on designing functionally graded heterogeneous stochastic implants by spatially changing unit cell size, strut thickness, and porosity [23,24]. To design stochastic models with controlled properties, a new Voronoi method is introduced based on a top-down design approach and probability spheres. In the proposed models the porosity of the stochastic structure could gradually change laterally, which was illustrated by the graded distribution of pore spheres [23,25]. Gradient mechanical properties can also be achieved by varying the laser parameters during the AM process resulting in struts with various thicknesses distribution [26]. Bone-like stochastic structures can also be inspired by the native bone tissue. In a study, the 3D STL model of the implants was reconstructed from the computed tomography (CT) scanning data of the stochastic bone tissue and imported to a 3D printing system for prototyping [27]. Finding the optimal distribution of the seeding points based on the CT data from bone tissue is the main objective of this class of research.

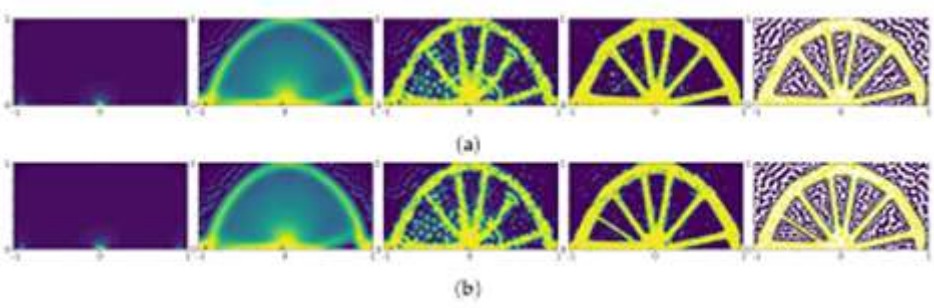

Fig-6 Stochastic topologies optimisation under uncertainties

1.5.2 Lattice networks

Lattice structures are the complex architectures consist of an array of interconnected struts or plates that are repeatedly aligned in the 3D space [28,29]. The lattice structure within the metal implant formed within the metal implant match its mechanical properties very close to the surrounding hard tissue. Besides, lattice structures pose an interconnected pore architecture promotes the cell ingrowth and better tissue integration. Some well-known lattice topologies include cubic, octahedron, and truncated as demonstrated. The Lattice structures of simple geometries have been manufactured using traditional fabrication techniques like water jet cutting, casting, electroless plating, and electrodeposition [30]. These old techniques are very time-consuming, costly, and unable to fabricate high-resolution complex structures. The AM techniques for metal came into existence recently as the solution of all former difficulties, one can fabricate thin struts and lattice geometries in high resolutions and complex shapes with a lower cost and less time consuming [31]. Although the optimized target is not achieved the manufactured structure by CAD models due to some limitations in metal AM, it is so

small that can be ignored or can be rectified by post processing and the experimental data can be validated by simulation [32,33]. The Lattice structures are modeled by various CAD software likeSolid works, Meshmixer, MATLAB, etc., to create STL files for AM [34,35]. Modeling of lattice networks allows the design of scaffolds across the full range of relative density (zero to 100%) without losing interconnectivity. The physical properties of lattice-based structures strongly depend on the design of pore characteristics (pore size, pore shape, and relative density) [36]. In terms of porosity, it is evident that the permeability is enhanced with porosity, whereas compressive strength and elastic modulus are inversely proportional to porosity [37]. The mechanical properties of lattice struts are correlated to their mechanism of failure. For instance, cube and truncated cube unit cell types are classified as stretching-dominated structures where compressive failure is dominated by a layer-by-layer collapse mechanism. In these structures, the internal linkages are oriented along with the loading direction. On the contrary, unit cell types such as diamond consist of diagonal struts angled relative to the loading direction. These structures are referred to as bending-dominated architectures wherein the compressive failure is typically originated from progressive shear bands across the porous structure. In general, bending-dominated pore shapes are characterized with lower elastic modulus and compressive strength compared to that of stretching-dominated structures [38]. This behavior is attributed to the generally larger strength of metals under axial versus shear deformations. The larger strength of cubic pore share relative to the diamond was also confirmed both experimentally and numerically using finite element simulations on Ti-based scaffolds [38]. The permeability of the porous structures with lower relative densities was more sensitive to the pore shape [11]. The conventional bulk materials as well as most lattice structures, are typically characterized with a positive Poisson's ratio. A recent trend in the literature emphasizes the auxetic metamaterials (negative Poisson's ratio), where the structure transversely shrinks when subjected to compressive loads. Auxetic porous structures have provided many opportunities for the design of porous implant structures.

1.5.3 Triply periodic minimal surfaces (TPMS)

TPMS are smooth infinite tortuous surfaces with zero mean curvature that divides the 3D space into two continuous phases [39]. It allows for tuning the mechanical properties to match theimplant with the host tissue like lattice architectures and also tissue ingrowth for better integrity and durability. Different varieties of pore shapes, porosity, and unit cell sizes can be mathematically defined and applied to each unit cell, that can be patterned along the global axes [40]. The TPMS geometries can be defined by the generalized Equation:

$\Gamma(r) = \sum_{l=1}^{L} \sum_{M=1}^{M} \mu_{lm} \cos(2\pi k_l (P_{m.}^{T} . r)) = C$

Where P_m =[$a_m, b_m, c_m]^T$ is the basic vector in 3D

r= $[x, y, r]^T$indicates the location vector

k_l =Scale parameter

μ_{lm} = Periodic moment

The left side of Equation dictates the topology of the unit cells. The constant C (offset value) in the rightside of the equation controls the relative density (in the case of solid network TPMS structures) [41]. To design scaffolds, φ < C or φ > C defines the solid phase for solid network TPMS types. One major limitation in solid network TPMS structures involves the lack of interconnectivity at the extreme design relative densities as the TPMS structures lose their continuousness at those ranges of offset values (C) [42,43]. Sheet networks can be defined either by thickening the TPMS surfaces or defining –C < φ < C as the solid phase [44] .

Based on the above general equation, the equations corresponding to P-, D-, and G-surface topologies can be obtained as

ΓP(r) = cos x + cos y + cos z = C and

ΓD(r) = cos x cos y cos z − sin x sin y sin z = C, and

ΓG(r) = sin x cos y + sin y cos z + sin z cos x,

Industrial Engineering Journal
ISSN: 0970-2555
Volume : 52, Issue 3, March : 2023

The typical commercial modelling software such as SolidWorks, and CATIA lack specific modules for modelling mathematically defined patterned surfaces. Modelling massive TPMS structures containing a high number of unit cells is also computationally expensive. Hence, the CAD design of TPMS scaffolds has entailed auxiliary computer programs that work based on point clouds, and image processing approaches [45]. Similar to lattice networks, not only pore shape, but also relative density and specific surface area can be engineered to tune the mechanical properties in TPMS designs [46]. The failure mechanism of the TPMS structures can be characterized by either 45◦ shear band formation (mostly in bending dominated structures) or layer-by-layer collapse (mostly in stretching dominated structures) [47,48]. Typical compressive stress-strain curves for these structures follow that of typical porous materials where it begins with an elastic linear region followed by fluctuations corresponding to the progressive failure of the internal layers. The cubical strut-based lattices with straight struts and sharp turns and corners (without uniform transition surfaces) show poor manufacturability in the AM processes (especially for the horizontal struts in large unit cell sizes and low volume fractions). These features can also result in thermal deformation in long overhanging features. TPMS structures enhanced additive manufacturability due to their smooth surfaces and uniform curvatures that can allow their self-supporting manufacturing [49]. Besides, cubical strut-based lattices with sharp corners show higher stress concentration compared to TPMS scaffolds with smooth curvy surfaces [50,51]. The superior mechanical and biological properties of the TPMS structures compared to that of lattice structures have been reported in the literature [52–55]. In a study by Davar Ali et al. [206], TPMS-based scaffolds showed higher permeability compared to lattice structures and the maximum wall shear stress (WSS) was attributed to the lattice structures. Besides, the in vitro studies confirmed that the open, interconnected TPMS structures show improved cell ingrowth compared to the scaffolds fabricated by traditional salt leaching (stochastic design) [56,207].

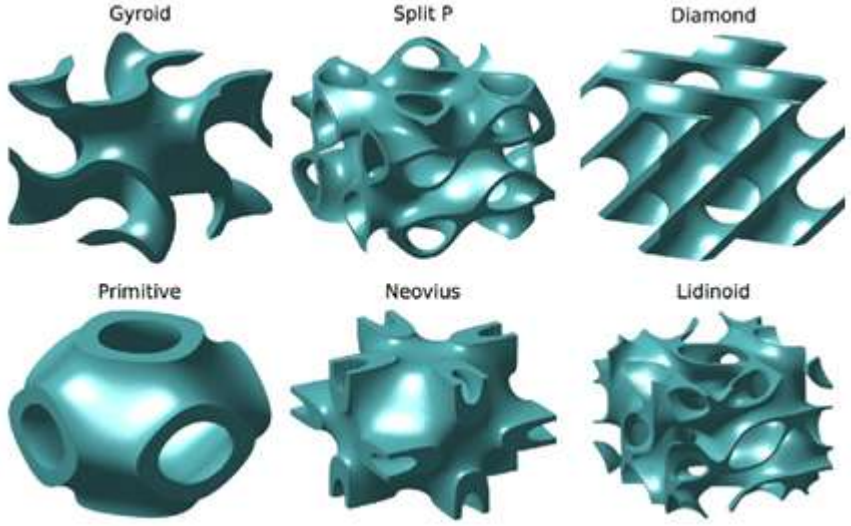

Conclusion: -

This manuscript presents about the basic ideas about various topological optimization aspects implemented in AM for the implant fabrication. The mathematical simulation transforms density maps into manufacturable surface lattice structure. The result is simulation creates surface lattice domain effectively resemble the given density map and can be fabricated using

AM. The network phase lattice structure has been limitation to map small density values due to the generation of disconnections in the boundary of the cells. The matrix phase structures have the capacity to map along the range of densities. The minimum density that can be represented is dictated by the manufacturing technology and the limitation associated with the machine.

References: -

[1] Bendsoe, M. P., and Sigmund, O., "Material interpolation schemes in topology optimization," Archive of Applied Mechanics, 69 (9-10), 635-654, 1999.
[2] Vahdat, S. E. "AlirezaPournaghi, Optimization of Bone Implant Selection with Price Analysis." International journal of Advanced Materials Manufacturing & Characterization 3 (2013): 37-46.
[3] Liou, Frank W. Rapid prototyping and engineering applications: a toolbox for prototype development. CRC Press, 2007.
[4] M. Zhou, G.I.N. Rozvany, The COC algorithm, Part II: topological, geometrical and generalized shape optimization, Compute. Methods Appl. Mech. Eng. 89 (1991) 309–336
[5] T. Iqbal, L. Wang, D. Li, E. Dong, H. Fan, J. Fu, C. Hu, A general multi-objective topology optimization methodology developed for customized design of pelvic prostheses, Med. Eng. Phys. 69 (2019) 8–16.
[6] M.A. Al-Ali, M.A. Al-Ali, A. Takizawa, M. Kitamura, Topology optimization and fatigue analysis of temporomandibular joint prosthesis, World J. Mech. (2017) 323–339, 07
[7] J. Wu, N. Aage, R. Westermann, O. Sigmund, Infill optimization for additive manufacturing-approaching bone-like porous structures, IEEE Trans. Visual. Comput. Graph. 24 (2018) 1127–1140.
[8] J. Park, A. Sutradhar, J.J. Shah, G.H. Paulino, Design of complex bone internal structure using topology optimization with perimeter control, Comput. Biol. Med. 94 (2018) 74–84.
[9] C. Pan, Y.F. Han, J.P. Lu, Design and optimization of lattice structures: a review, Appl. Sci. 10 (2020), 6374
[10] F. Tamburrino, S. Graziosi, M. Bordegoni, The design process of additively manufactured mesoscale lattice structures: a review, J. Comput. Inf. Sci. Eng. 18 (2018), 040801
[11] W. Tao, M.C. Leu, in: Design of Lattice Structure for Additive Manufacturing, 2016 International Symposium on Flexible Automation (ISFA), IEEE, 2016, pp. 325–332.
[12] K.F. Leong, C.M. Cheah, C.K. Chua, Solid freeform fabrication of three-dimensional scaffolds for engineering replacement tissues and organs, Biomaterials 24 (2003) 2363–2378.
[13] H. Lo, M.S. Ponticiello, K.W. Leong, Fabrication of controlled release biodegradable foams by phase separation, Tissue Eng. 1 (1995) 15–28.
[14] A.G. Mikos, G. Sarakinos, S.M. Leite, J.P. Vacant, R. Langer, Laminated three-dimensional biodegradable foams for use in tissue engineering, Biomaterials 14 (1993) 323–330
[15] H. Montazerian, M. Zhianmanesh, E. Davoodi, A.S. Milani, M. Hoorfar, Longitudinal and radial permeability analysis of additively manufactured porous scaffolds: effect of pore shape and porosity, Mater. Des. 122 (2017) 146–156.
[16] M. Zhianmanesh, M. Varmazyar, H. Montazerian, Fluid permeability of graded porosity scaffolds architectured with minimal surfaces, ACS Biomater. Sci. Eng. 5 (2019) 1228–1237.
[17] M. Fantini, M. Curto, Interactive design and manufacturing of a voronoi-based biomimetic bone scaffold for morphological characterization, Int. J. Interact. Des. 12 (2018) 585–596.
[18] H. Chen, Y. Liu, C. Wang, A. Zhang, B. Chen, Q. Han, J. Wang, Design and properties of biomimetic irregular scaffolds for bone tissue engineering, Comput. Biol. Med. 130 (2021), 104241.
[19] H. Chen, Q. Han, C. Wang, Y. Liu, B. Chen, J. Wang, Porous scaffold design for additive manufacturing in orthopedics: a review, Front. Bioeng. Biotechnol. 8 (2020) 609
[21] T. Liu, S. Guessasma, J.H. Zhu, W.H. Zhang, Designing cellular structures for additive manufacturing using Voronoi-Monte Carlo approach, Polymers 11 (2019) 1158.
[22] G. Savio, S. Rosso, R. Meneghello, G. Concheri, Geometric modeling of cellular materials for additive manufacturing in biomedical field: a review, Appl. Bionics Biomechanics 2018 (2018), 1654782
[23] G. Wang, L. Shen, J. Zhao, H. Liang, D. Xie, Z. Tian, C. Wang, Design and compressive behavior of controllable irregular porous scaffolds: based on voronoi-tessellation and for additive manufacturing, ACS Biomater. Sci. Eng. 4 (2018) 719–727.

[24] Y. Du, H.X. Liang, D.Q. Xie, N. Mao, J.F. Zhao, Z.J. Tian, C.J. Wang, L.D. Shen, Design and statistical analysis of irregular porous scaffolds for orthopedic reconstruction based on Voronoi tessellation and fabricated via selective laser melting (SLM), Mater. Chem. Phys. 239 (2020), 121968
[25] H.Y. Lei, J.R. Li, Z.J. Xu, Q.H. Wang, Parametric design of voronoi-based lattice porous structures, Mater. Des. 191 (2020), 108607.
[26] S. Ghouse, N. Reznikov, O.R. Boughton, S. Babu, K.C. Geoffrey Ng, G. Blunn, J. P. Cobb, M.M. Stevens, J.R.T. Jeffers, The design and in vivo testing of a locally stiffness-matched porous scaffold, Appl. Mater. Today 15 (2019) 377–388
[27] M.M. Barak, M.A. Black, A novel use of 3D printing model demonstrates the effects of deteriorated trabecular bone structure on bone stiffness and strength, J. Mech. Behav. Biomed. Mater. 78 (2018) 455–464.
[28] R.M. Gorguluarslan, U.N. Gandhi, R. Mandapati, S.-K. Choi, Design and fabrication of periodic lattice-based cellular structures, Comput. Aided Des. Appl. 13 (2016) 50–62
[29] T.A. Schaedler, W.B. Carter, Architected cellular materials, Annu. Rev. Mater. Res. 46 (2016) 187–210
[30] M. Helou, S. Kara, Design, analysis and manufacturing of lattice structures: an overview, Int. J. Comput. Integrated Manuf. 31 (2018) 243–261
[31] C. Pan, Y.F. Han, J.P. Lu, Design and optimization of lattice structures: a review, Appl. Sci. 10 (2020), 6374.
[32] M. Zhianmanesh, M. Varmazyar, H. Montazerian, Fluid permeability of graded porosity scaffolds architectured with minimal surfaces, ACS Biomater. Sci. Eng. 5 (2019) 1228–1237.
[33] A. Bandyopadhyay, Y. Zhang, S. Bose, Recent developments in metal additive Manufacturing, curr. Opin. Chem, Eng. 28(2020) 96-104
[34] M. McMillan, M. Jurg, M. Leary, M. Brandt, Programmatic lattice generation for additive manufacture, in: Proceedings of the 1st International Design Technology Conference, Destech2015, 2015, pp. 178–184
[35] N.A. Meisel, C.B. Williams, A. Druschitz, Lightweight metal cellular structures via indirect 3D printing and casting, in: Proceedings of the International Solid Freeform Fabrication Symposium, 2012, pp. 162–176
[36] C. Lu, M.X. Qi, S. Islam, P. Chen, S.S. Gao, Y.R. Xu, X.D. Yang, Mechanical performance of 3D-printing plastic honeycomb sandwich structure, Int. J. Precis. Eng. Manuf. 5 (2018) 47–54.
[37] Y. Du, H.X. Liang, D.Q. Xie, N. Mao, J.F. Zhao, Z.J. Tian, C.J. Wang, L.D. Shen, Finite element analysis of mechanical behavior, permeability of irregular porous scaffolds and lattice-based porous scaffolds, Mater. Res. Express 6 (2019), 105407.
[38] H.M.A. Kolken, C.P. de Jonge, T. van der Sloten, A.F. Garcia, B. Pouran, K. Willemsen, H. Weinans, A.A. Zadpoor, Additively manufactured space-filling meta-implants, ActaBiomater. 125 (2021) 345–357
[39] Y. Yang, G. Wang, H. Liang, C. Gao, S. Peng, L. Shen, C. Shuai, Additive manufacturing of bone scaffolds, Int. J. Bioprinting 5 (2019) 148
[40] J. Shi, L. Zhu, L. Li, Z. Li, J. Yang, X. Wang, A TPMS-based method for modeling porous scaffolds for bionic bone tissue engineering, Sci. Rep. 8 (2018) 7395
[41] E. Davoodi, H. Montazerian, R. Haghniaz, A. Rashidi, S. Ahadian, A. Sheikhi, J. Chen, A. Khademhosseini, A.S. Milani, M. Hoorfar, E. Toyserkani, 3D-Printed ultra-robust surface-doped porous silicone sensors for wearable biomonitoring, ACS Nano 14 (2020) 1520–1532
[42] E. Davoodi, H. Montazerian, A. Khademhosseini, E. Toyserkani, Sacrificial 3D printing of shrinkable silicone Elastomers for enhanced feature resolution in flexible tissue scaffolds, ActaBiomater. 117 (2020) 261–272.
[43] M.R. Mansouri, H. Montazerian, S. Schmauder, J. Kadkhodapour, 3D-Printed multimaterial composites tailored for compliancy and strain recovery, Compos. Struct. 184 (2018) 11–17

[44] O. Al-Ketan, D.W. Lee, R. Rowshan, R.K. Abu Al-Rub, functionally graded and multi-morphology sheet TPMS lattices: design, manufacturing, and mechanical properties, J. Mech. Behav. Biomed. Mater. 102 (2020), 103520.
[45] H. Montazerian, M.G.A. Mohamed, M.M. Montazeri, S. Kheiri, A.S. Milani, K. Kim, M. Hoorfar, Permeability and mechanical properties of gradient porous PDMS scaffolds fabricated by 3D-printed sacrificial templates designed with minimal surfaces, ActaBiomater. 96 (2019) 149–160
[46] S. Vijayavenkataraman, L. Zhang, S. Zhang, J.Y.H. Fuh, W. Feng, triply periodic minimal surfaces sheet scaffolds for tissue engineering applications: an optimization approach toward biomimetic scaffold design, ACS Appl. Bio Mater. 1 (2018) 259–269.
[47] J. Kadkhodapour, H. Montazerian, S. Raeisi, investigating internal architecture effect in plastic deformation and failure for TPMS-based scaffolds using simulation methods and experimental procedure, Mater. Sci. Eng. C 43 (2014) 587–597.
[48] J. Kadkhodapour, H. Montazerian, A.C. Darabi, A. Zargarian, S. Schmauder, the relationships between deformation mechanisms and mechanical properties of additively manufactured porous biomaterials, J. Mech. Behav. Biomed. Mater. 70 (2017) 28–42.
[49] L. Yang, C.Z. Yan, C.J. Han, P. Chen, S.F. Yang, Y.S. Shi, Mechanical response of a triply periodic minimal surface cellular structures manufactured by selective laser melting, Int. J. Mech. Sci. 148 (2018) 149–157.
[50] R. Ambu, A.E. Morabito, Porous scaffold design based on minimal surfaces: development and assessment of variable architectures, Symmetry 10 (2018) 361.
[51] O. Al-Ketan, R. Rezgui, R. Rowshan, H. Du, N.X. Fang, R.K. Abu Al-Rub, Microarchitected stretching-dominated mechanical metamaterials with minimal surface topologies, Adv. Eng. Mater. 20 (2018), 1800029.
[52] D.W. Abueidda, M. Bakir, R.K. Abu Al-Rub, J.S. Bergstrom, N.A. Sobh, I. Jasiuk, Mechanical properties of 3D printed polymeric cellular materials with triply periodic minimal surface architectures, Mater. Des. 122 (2017) 255–267.
[53] D.W. Abueidda, M. Elhebeary, C.S. Shiang, S.Y. Pang, R.K. Abu Al-Rub, I. M. Jasiuk, Mechanical properties of 3D printed polymeric gyroid cellular structures: experimental and finite element study, Mater. Des. 165 (2019), 107597.
[54] S.C. Han, J.W. Lee, K. Kang, A new type of low-density material: shellular, Adv. Mater. 27 (2015) 5506–5511.
[55] M.G. Lee, J.W. Lee, S.C. Han, K. Kang, Mechanical analyses of "shellular", an ultralow-density material, Acta Mater. 103 (2016) 595–607.
[56] S.X. Yu, J.X. Sun, J.M. Bai, Investigation of functionally graded tpms structures fabricated by additive manufacturing, Mater. Des. 182 (2019), 108021
[57] S.X. Yu, J.X. Sun, J.M. Bai, Investigation of functionally graded tpms structures fabricated by additive manufacturing, Mater. Des. 182 (2019), 10802